

Enhanced thermoelectric properties in two-dimensional monolayer Si_2BN by adsorbing halogen atoms

Cheng-Wei Wu(吴成伟), Changqing Xiang(向长青), Hengyu Yang(杨恒玉), Wu-Xing Zhou(周五星), Guofeng Xie(谢国锋), Baoli Ou(欧宝立), and Dan Wu(伍丹)

Citation: Chin. Phys. B, 2021, 30 (**3**): 037304. DOI: 10.1088/1674-1056/abd163
Journal homepage: http://cpb.iphy.ac.cn; http://iopscience.iop.org/cpb

What follows is a list of articles you may be interested in

Tunable metal-insulator transition in $LaTiO_3/CaVO_3$ superlattices: A theoretical study

Ya-Kui Weng(翁亚奎), Meng-Lan Shen(沈梦兰), Jie Li(李杰), and Xing-Ao Li(李兴鳌)
Chin. Phys. B, 2020, 29 (**12**): 127303. DOI: 10.1088/1674-1056/abc237

Electronic and thermoelectric properties of alkali metal-based perovskites $CsYbF_3$ and $RbYbF_3$

Q Mahmood, N A Noor, T Ghrib, Nessrin A Kattan, Asif Mahmood, and Shahid M Ramay
Chin. Phys. B, 2020, 29 (**11**): 117305. DOI: 10.1088/1674-1056/ab9de3

Artificial neural network potential for gold clusters

Ling-Zhi Cao(曹凌志), Peng-Ju Wang(王鹏举), Lin-Wei Sai(赛琳伟), Jie Fu(付洁), and Xiang-Mei Duan(段香梅)
Chin. Phys. B, 2020, 29 (**11**): 117304. DOI: 10.1088/1674-1056/abc15d

Epitaxial fabrication of monolayer copper arsenide on Cu(111)

Shuai Zhang(张帅), Yang Song(宋洋), Jin Mei Li(李金梅), Zhenyu Wang(王振宇), Chen Liu(刘晨), Jia-Ou Wang(王嘉鸥), Lei Gao(高蕾), Jian-Chen Lu(卢建臣), Yu Yang Zhang(张余洋), Xiao Lin(林晓), Jinbo Pan(潘金波), Shi Xuan Du(杜世萱), Hong-Jun Gao(高鸿钧)
Chin. Phys. B, 2020, 29 (**7**): 077301. DOI: 10.1088/1674-1056/ab8db3

Tailoring electronic properties of two-dimensional antimonene with isoelectronic counterparts

Ye Zhang(张也), Huai-Hong Guo(郭怀红), Bao-Juan Dong(董宝娟), Zhen Zhu(朱震), Teng Yang(杨腾), Ji-Zhang Wang(王吉章), Zhi-Dong Zhang(张志东)
Chin. Phys. B, 2020, 29 (**3**): 037305. DOI: 10.1088/1674-1056/ab6c4e

---

SPECIAL TOPIC — Phononics and phonon engineering

Enhanced thermoelectric properties in two-dimensional monolayer Si_2BN by adsorbing halogen atoms*

Cheng-Wei Wu(吴成伟)[1], Changqing Xiang(向长青)[2], Hengyu Yang(杨恒玉)[1], Wu-Xing Zhou(周五星)[1,†], Guofeng Xie(谢国锋)[1], Baoli Ou(欧宝立)[1], and Dan Wu(伍丹)[3,‡]

[1] School of Materials Science and Engineering & Hunan Provincial Key Laboratory of Advanced Materials for New Energy Storage and Conversion, Hunan University of Science and Technology, Xiangtan 411201, China

[2] College of Information Science and Engineering, Jishou University, Jishou 416000, China

[3] School of Physics and Electronic Science, Changsha University of Science and Technology, Changsha 410114, China

(Received 30 September 2020; revised manuscript received 4 December 2020; accepted manuscript online 8 December 2020)

Using the first principles calculation and Boltzmann transport theory, we study the thermoelectric properties of Si_2BN adsorbing halogen atoms (Si_2BN-4X, X = F, Cl, Br, and I). The results show that the adsorption of halogen atoms can significantly regulate the energy band structure and lattice thermal conductivity of Si_2BN. Among them, Si_2BN-4I has the best thermoelectric performance, the figure of merit can reach 0.50 K at 300 K, which is about 16 times greater than that of Si_2BN. This is because the adsorption of iodine atoms not only significantly increases the Seebeck coefficient due to band degeneracy, but also rapidly reduces the phonon thermal conductivity by enhancing phonon scattering. Our work proves the application potential of Si_2BN-based crystals in the field of thermoelectricity and the effective method for metal crystals to open bandgaps by adsorbing halogens.

Keywords: density functional theory, thermoelectric effects, transport properties, electronic structure

PACS: 71.15.−m, 73.50.Lw, 74.25.F−, 74.25.Jb **DOI:** 10.1088/1674-1056/abd163

1. Introduction

Thermoelectric (TE) materials can directly convert waste heat into electricity and vice versa, which provide an effective way for the solution of the global energy crisis without producing new contaminants.[1–3] TE materials have attracted intense research efforts due to the huge demand for energy harvesting and power generation. The TE efficiency of the material is measured by the dimensionless figure of merit, $ZT = S\sigma^2 T/(\kappa_e + \kappa_p)$, where T is the temperature, S is the Seebeck coefficient, σ is the electrical conductivity, κ_e is the electronic thermal conductivity, and κ_p is the phonon thermal conductivity.[4–7]

According to the formula, high Seebeck coefficient S, high electrical conductivity σ, low phonon thermal conductivity κ_p can obtain high ZT.[8] However, these physical parameters S, σ, and κ_e are dependent on each other, e.g., the Wiedemann–Franz law indicates $\sigma \propto \kappa_e$, which causes the TE efficiency to be relatively low. Although the theoretical studies have showed that low-dimensional nanoscale systems can contribute to boosting the TE performance originated from the enhancement of phonon scattering and quantum confinement effect, the ZT of most perfect structures is still low because of their high thermal conductivity, such as graphene (2876 W/m·K),[9] borophene (κ_{zig} = 72 W/m·K, κ_{arm} = 145 W/m·K),[10] MoS_2 (κ_{zig} = 54 W/m·K, κ_{arm} = 33 W/m·K),[11] etc. Therefore, it is necessary to find appropriate means to reduce phonon transport to improve the TE performance. What is more, the TE parameter κ_p is the relatively independent quantity that can be changed by some method.[12–18]

In recent years, the thermal transport of low-dimensional nanomaterials has become a research hotspot. Theoretically, by manipulating the phonons or elastic waves that propagate and scatter, the beneficial thermal transport properties can be obtained. Research shows that surface functionalization is one of the feasible and effective manipulation methods.[19,20] This method has been used to regulate the thermal transfer of nanostructured materials composed of group-IV and group-V nonmetallic elements. For example, Wang *et al.*[21] reduced the thermal conductivity of graphene by depositing gold nanoparticles on its surface by physical deposition. The decrease of the thermal conductivity is mainly attributed to the suppression of ZA phonon modes. Liu *et al.*[22] improved the thermal conductivity of silene system by full hydrogenation. Although full hydrogenation increases the buckling degree of the silene system, the elimination of asymmetric π-bond is considered to be the main reason for the decrease of phonon scattering rate and the increase of thermal conductivity of hy-

*Project supported by the National Natural Science Foundation of China (Grant Nos. 12074115, 11874145, and 51775183) and the Hunan Provincial Natural Science Fund of China (Grant No. 2018JJ2125).

†Corresponding author. E-mail: wuxingzhou@hnu.edu.cn

‡Corresponding author. E-mail: danwu@csust.edu.cn

© 2021 Chinese Physical Society and IOP Publishing Ltd

drogenated silene. Sun *et al.*[23] studied the effect of oxygen-containing functional groups on the thermal conductivity of reduced graphene oxide by molecular dynamics simulation. Overall, these results are all attributable to the effect of sp^3 hybridization introduced by surface functionalization on the material.

Moreover, surface functionalization not only can change the heat transport, but also can change the electron transport properties. For example, Xu *et al.*[24] reported that monolayer C_4N functionalization with adsorbing Li, Na, Be, Mg, Ti, V, Cr, and Mn atoms, resulting in the transformation of C_4N from semi-metal to semiconductor. By the first principles calculation, Nguyen *et al.*[25] found that the bandgap can be opened when the concentration of halogen atoms adsorbed on both sides of silicon is greater than 0.25. Therefore, surface functionalization is an effective way to improve the performance of two-dimensional (2D) materials in a specific field. Particularly, halogen atoms have strong electronegativity, which can bind free electrons on the surface of 2D materials and play a role of surface passivation. In order to open the bandgap of 2D materials with metal or semi-metallic properties, halogen is a good adsorption candidate.[26]

Si_2BN, which was reported by Andriotis *et al.* in 2016, is also a kind of graphene-like monolayer structure.[27] It has attracted the interest of researchers in hydrogen storage, battery, and other fields,[28–31] but there have been no reports of any research on TE properties. Because the crystalline structure of Si_2BN is more complex than graphene, we predict that it has lower phonon thermal conductivity, which is beneficial to the improvement of TE properties. Nevertheless, the electronic energy band of Si_2BN shows its routing metal property, this is negative for TE properties. In theory, by adsorbing halogen atoms on Si_2BN, the hybrid type changes from sp^2 to sp^3, resulting in bandgap opening.[32] Moreover, it also breaks the plane structure of Si_2BN, the lattice thermal conductivity is further reduced by increasing phonon scattering.

In this work, we research the thermoelectric transport properties of Si_2BN adsorbing halogen atoms (Si_2BN-4X, X = F, Cl, Br, and I) by using the first principles calculation and Boltzmann transport theory. By adsorbing halogen atoms, the band gap of Si_2BN is opened, which leads to the increase of the Seebeck coefficient. In particular, Si_2BN-4I has the largest Seebeck coefficient because of the band degeneracy. In addition, the absorption of halogen atoms increases the phonon scattering, and the lattice thermal conductivity decreases significantly, which leads to a significant increase in the thermoelectric properties.

2. Methodology

First-principles calculations are performed based on density functional theory (DFT) using the Vienna *ab-initio* simulation package (VASP).[33,34] We choose the generalized gradient approximation (GGA) in the Perdew–Burke–Ernzerhof (PBE) parametrization for the exchange–correlation functional.[35] The crystal structure is relaxed with total energy convergence criterion of 10^{-6} eV, the force convergence criterion is 10^{-4} eV/Å, and adopts plane-wave basis with kinetic energy cutoff of 500 eV. The $11\times11\times1$ Γ-center k-mesh is used, and the normal vacuum distance is large than 15 Å to prevent any physical interactions between the consecutive layers. VASP is used to obtain the second-order interatomic force constant by the finite displacement method with $3\times3\times1$ supercell and $1\times1\times1$ k-mesh, and then the dynamic matrix is constructed by the Phonopy program, and the dynamic matrix is diagonalized to obtain the phonon spectrum.[36]

Based on Boltzmann transport theory, we use VASP combined with BoltzTraP program to calculate the electronic transport properties of materials.[37] The TE transport parameters are calculated using the relaxation time approximation method, where the relaxation time constant τ is 10^{-14} s. This constant has been widely used in the calculation of electron transport properties and reliable results have been obtained.[38,39] Moreover, the TE transport coefficient is converged by using the k-mesh of $20\times20\times1$ in the Brillouin zone (BZ).[40,41]

We calculate the phonon thermal conductivity based on linearized phonon Boltzmann transport equation (PBTE) within relaxation time approximation.[42,43,45] Along the specified direction, the thermal conductivity of monolayer Si_2BN and its halide in each branch λ can be described as

$$\kappa_\lambda = \frac{S}{(2\pi)^2}\int c_{\rm ph} v_\lambda^2 \tau_\lambda \,{\rm d}q, \tag{1}$$

where S is the area of the sample, v_λ is the phonon group velocity of λ branch along the specified direction, which is equal to ${\rm d}\omega/{\rm d}q$, ω is the phonon frequency for branch λ at wave vector q, τ_λ is the phonon relaxation time of λ branch, and $c_{\rm ph}$ is the volumetric specific heat of each mode, which can be calculated with the following formula:

$$c_{\rm ph} = \frac{k_{\rm B}}{Sd}\cdot\frac{(\hbar\omega/k_{\rm B}T)^2\,{\rm e}^{\hbar\omega/k_{\rm B}T}}{({\rm e}^{\hbar\omega/k_{\rm B}T}-1)^2}. \tag{2}$$

Here $k_{\rm B}$ is the Boltzmann constant, $\hbar$ is the reduced Planck constant, d is the effective layer thickness of monolayer Si_2BN and its halide, and T is the absolute temperature.[46] The phonon relaxation time τ_λ can be obtained by the Matthiessen's rule, which can be written as

$$1/\tau_\lambda = 1/\tau_\lambda^{\rm U} + 1/\tau_\lambda^{\rm B}, \tag{3}$$

where $1/\tau_\lambda^{\rm U}$ and $1/\tau_\lambda^{\rm B}$ are the Umklapp phonon–phonon scattering rate and boundary scattering rate, respectively. In this

work, $1/\tau_\lambda^{\mathrm{B}}$ is not considered in the 2D system and $1/\tau_\lambda^{\mathrm{U}}$ can be given as[47,48]

$$1/\tau_\lambda^{\mathrm{U}} = \frac{\gamma_\lambda k_{\mathrm{B}} T \omega^2}{M v_\lambda^2 \omega_{\mathrm{D},\lambda}}, \tag{4}$$

$$\gamma_\lambda = \frac{V_0 \mathrm{d}\omega_\lambda(V)}{\omega_\lambda \mathrm{d}V}, \tag{5}$$

where γ_λ, M, $\omega_{\mathrm{D},\lambda}$ are the Grüneisen parameter, the mass of unit cell, and the Debye frequency of branch λ, respectively. V is the unit cell volume and V_0 is the completely relaxed unit cell volume. $\mathrm{d}\omega_\lambda(V)/\mathrm{d}V$ is the first derivative of the phonon frequency of branch λ with the volume.[49]

3. Results and discussion

Two optimized structures, named Si_2BN and Si_2BN-4X, are shown in Figs. 1(a) and 1(b), respectively. In top view of Fig. 1(a), the lattice constants of Si_2BN are $a = 6.35$ Å, $b = 6.45$ Å and the bond length between atoms are $l_{\mathrm{Si–Si}} = 2.24$ Å, $l_{\mathrm{Si–N}} = 1.76$ Å, $l_{\mathrm{Si–B}} = 1.95$ Å, and $l_{\mathrm{B–N}} = 1.46$ Å, which are in good agreement with the previously reported ones.[50] In side view of Fig. 1(a), the Si_2BN shows a plane structure, while the Si_2BN-4X (X = F, Cl, Br, I) shows the buckling structure when the surface of Si_2BN adsorbs halogen elements, as shown in the side view of Fig. 1(b), which is due to the change of the hybrid type of Si–Si atoms. The previous work pointed out that the buckling structure is more beneficial to increase phonon scattering and decrease phonon thermal conductivity.[51]

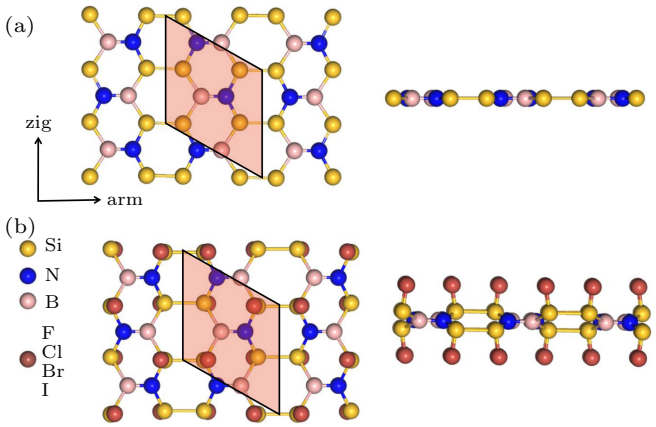


Fig. 1. Top and side views of the geometric structure of (a) Si_2BN and (b) Si_2BN-4X (X = F, Cl, Br, I).

In Fig. 2(a), the electronic band structure of Si_2BN presents a metal characteristic and the result matches that of Singh *et al.*[29] well. However, the materials with insulator or metal property are not good TE materials even though they have a large conductivity or Seebeck coefficient than semiconductor materials.

Therefore, a suitable method to open the bandgap for Si_2BN should be applied. When the halogen atoms are adsorbed on the four Si atoms of surface of Si_2BN (named Si_2BN-4X, X = F, Cl, Br, I), as shown in Fig. 3, the electronic structure property of Si_2BN transforms from metal to indirect bandgap semiconductor. In addition, the bandgap increases from 1.32 eV of Si_2BN-4F to 1.88 eV of Si_2BN-4I with the increase of atomic mass of adsorbed halogen, which is presented in Figs. 3(a)–3(d). It is worth mentioning that the electron band structure shows that Si_2BN-4X has flat conduction band minimum (CBM) and valence band maximum (VBM), indicating that it has high effective carrier mass, low carrier mobility, and low conductivity, which leads to high S eventually.[52] In addition, the degeneracy of the electronic band structure of Si_2BN-4I at the M point in BZ means a large S, which is beneficial to the improvement of ZT.[53–55]

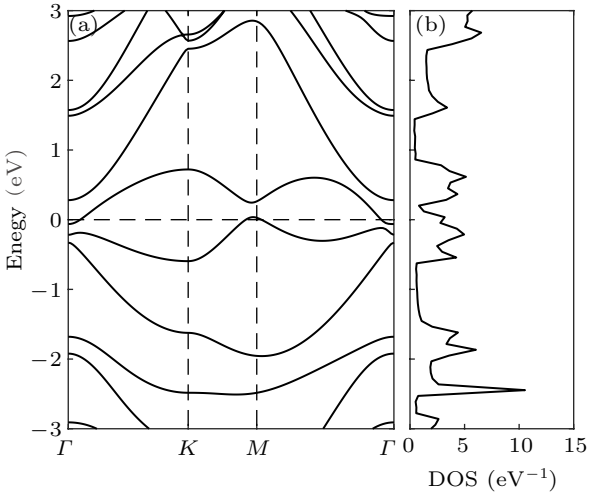


Fig. 2. (a) The electronic band structure and (b) DOS of Si_2BN.

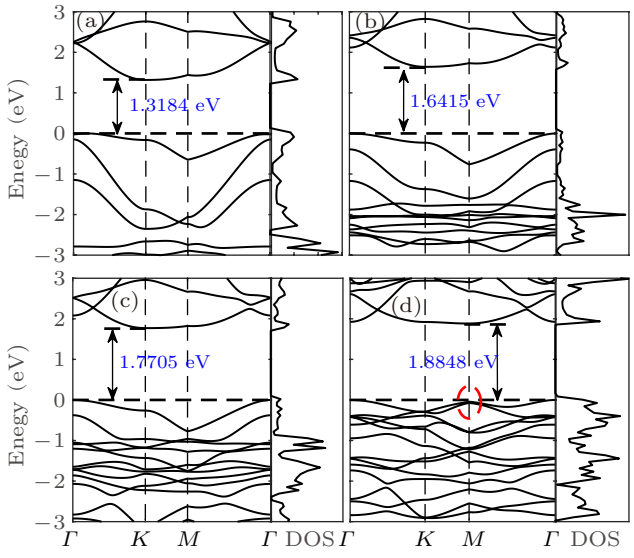


Fig. 3. The electronic band structure of (a) Si_2BN-4F, (b) Si_2BN-4Cl, (c) Si_2BN-4Br, (d) Si_2BN-4I.

In order to prove the dynamic stability of Si_2BN and Si_2BN-4X, we use the finite displacement method to calculate the phonon spectrum. In Fig. 4, the results show that there are no imaginary frequencies in the whole BZ, indicating the

dynamical stability of Si_2BN and Si_2BN-4X. In the phonon spectrums of Si_2BN and Si_2BN-4X, there are multiple phonon gaps in the frequency range from 15 THz to 40 THz. Besides, there are typical strong hybrid features between low-frequency optical branches and acoustic branches in Si_2BN and Si_2BN-4X. These characteristics indicate that the phonon thermal conductivity of Si_2BN and Si_2BN-4X will be relatively low. Importantly, as shown in Figs. 4(b)–4(e), there are more and more low-frequency flat optical branches from the Si_2BN-4F to Si_2BN-4I structure, which means that the phonon thermal conductivity will decrease with the increase of atomic mass of the absorbed halogen.[56]

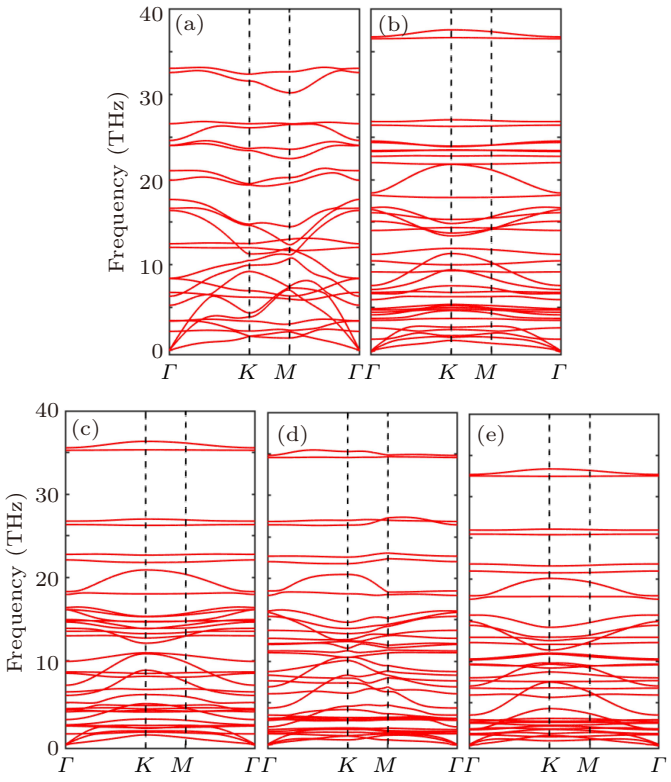


Fig. 4. The phonon dispersion spectra of (a) Si_2BN, (b) Si_2BN-4F, (c) Si_2BN-4Cl, (d) Si_2BN-4Br, (e) Si_2BN-4I.

On the other hand, in order to prove the thermodynamic stability of halogen atoms adsorbed Si_2BN, we calculate the adsorption formation energy of halogen atoms on Si_2BN surface as shown in Table 1. According to the definition of adsorption formation energy, the formula for our system can be written as

$$E_f = \left\{nE_b[Si_2BN\text{-}4X] - (n-n_X)E_b[Si_2BN] - n_X E_b[X_2]\right\}/n_X, \quad (6)$$

where $E_b[Si_2BN\text{-}4X]$, $E_b[Si_2BN]$, $E_b[X_2]$ are the bind energy per atom of Si_2BN-4X, the bind energy per atom of Si_2BN, and the bind energy per atom of X_2, respectively. n is the total number of Si_2BN-4X, n_X is the number of adsorbing halogen atoms. E_f is the adsorption formation energy per adsorbing halogen atom of Si_2BN-4X.

The unit adsorption formation energies of the X atom on the Si_2BN are all above 1 eV/atom as shown in Table 1. This means that the binding energy of Si_2BN-4X is larger, and the energy released by the formation of Si_2BN-4X from isolated atoms is greater than that of Si_2BN and X_2. Therefore, the lower total free energy of Si_2BN-4X demonstrates that the adsorption of X_2 by Si_2BN is experimentally feasible.

Table 1. The adsorption formation energy of halogen atoms adsorbed by Si_2BN is calculated. $E_f[Si_2BN\text{-}4X]$ is the adsorption formation energy per adsorbing halogen of Si_2BN-4X, $E_b[Si_2BN\text{-}4X]$ is the bind energy per atom of Si_2BN and Si_2BN-4X, and $E_b[X_2]$ is the bind energy per atom of X_2.

Si_2BN-4X	$E_b[X_2]$ (eV/atom)	$E_b[Si_2BN\text{-}4X]$ (eV/atom)	$E_f[Si_2BN\text{-}4X]$ (eV/atom)
Si_2BN-4F	1.63	5.23	4.02
Si_2BN-4Cl	1.723	4.56	1.92
Si_2BN-4Br	1.29	4.343	1.70
Si_2BN-4I	1.16	4.10	1.09
Si_2BN		5.02	

The Si_2BN and Si_2BN-4X have 2D hexagonal structures. We can study the TE properties along the armchair and zigzag directions. Firstly, we focus on the armchair direction. In order to systematically study the TE properties of Si_2BN and Si_2BN-4X along the armchair direction at room temperature, we calculate the Seebeck coefficient S, electrical conductivity σ, electronic thermal conductivity κ_e, power factor PF, phonon thermal conductivity κ_p, and ZT based on the average temperature T of 300 K and electron constant relaxation time τ of 10^{-14} s. All the results are plotted in Fig. 5. As shown in Figs. 5(a)–5(b), the S of Si_2BN-4X is larger than that of Si_2BN; moreover, S decreases and σ increases with the increase of charge carrier concentration n, which is due to the Pisarenko relation.[57] However, the PF of Si_2BN and Si_2BN-4X appear a maximum as n increases, and the maximal PF of the former is much lower than that of the latter, indicating that the optimal TE performance of Si_2BN-4X can be realized at some carrier concentration.

As can be seen from Fig. 5(d), the electronic thermal conductivity displays similar behavior to the conductivity. In addition, we can see that the phonon thermal conductivity of Si_2BN-4X is lower than that of Si_2BN in the temperature range from 200 K to 800 K, as illustrated in Fig. 5(e). It is worth noting that the phonon thermal conductivity κ_p of Si_2BN-4I is the lowest among all structures. According to the TE formula, we calculate the TE figure of merit as a function of carrier concentration, as shown in Fig. 5(f). The ZT values of Si_2BN-4X are significantly greater than that of Si_2BN, regardless of the change in carrier concentration. Meanwhile, the ZT curve of Si_2BN-4X increases firstly and then decreases with the increases of carrier concentration, where the ZT value of Si_2BN-4I is the largest compared to others structures. At 300 K, the ZT maximum of Si_2BN is only 0.03, while that of Si_2BN-4I reaches 0.50, which is about 16 times that of Si_2BN.

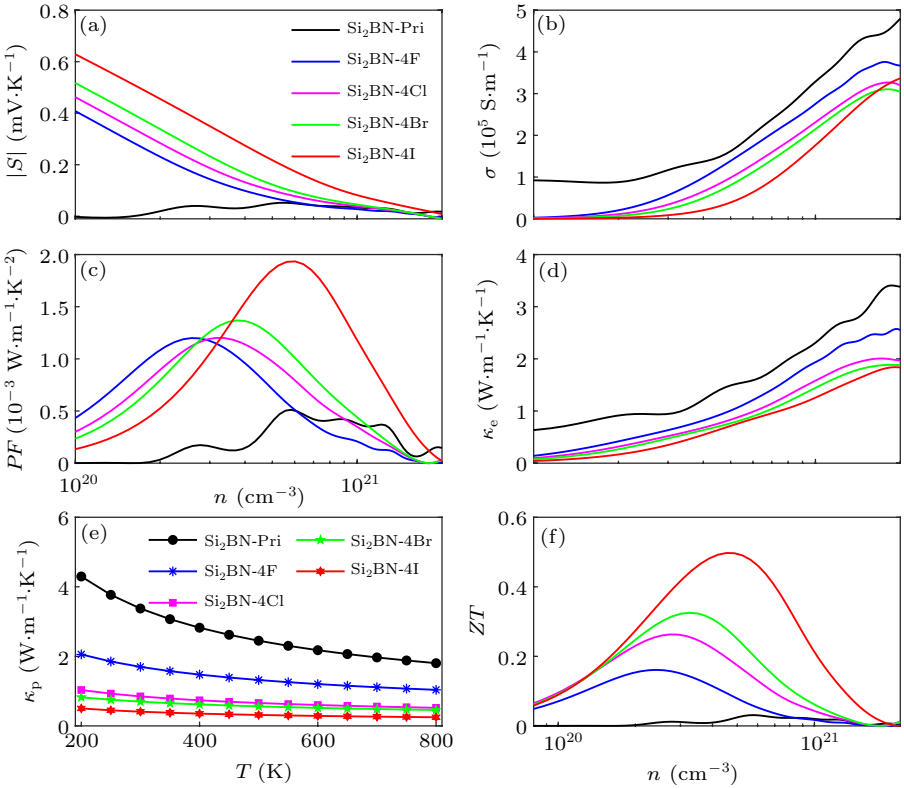


Fig. 5. (a) The Seebeck coefficient, (b) electrical conductivity, (c) power factor, (d) electronic thermal conductivity, (e) phonon thermal conductivity, and (f) ZT of Si_2BN and Si_2BN-4X along armchair direction.

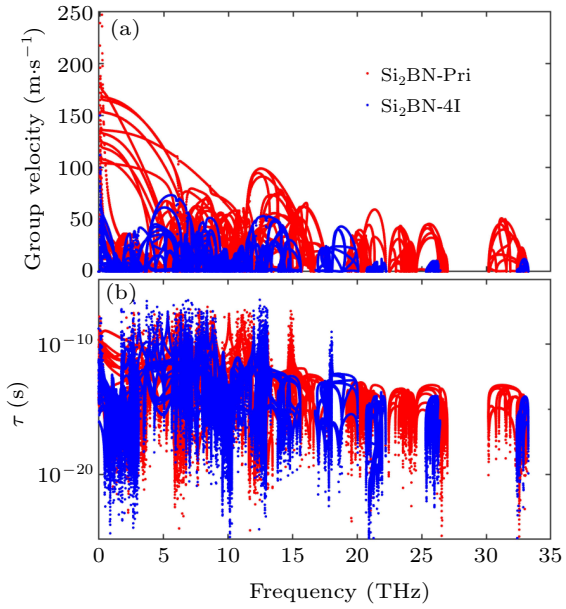


Fig. 6. (a) The group velocity and (b) phonon lifetime of Si_2BN-4I along armchair direction.

From the above results, Si_2BN-4I is the optimal structure for TE performance, which stems from the lowest thermal conductively after the surface functionalization. The phonon thermal conductivity of Si_2BN-4I is only 0.41 W/m·K while that of Si_2BN is 3.38 W/m·K at 300 K. In order to explain the decrease of phonon thermal conductivity of Si_2BN-4I compared with that of Si_2BN in armchair direction, we calculate the group velocity and phonon lifetime along the armchair direction. Figure 6(b) shows that the Si_2BN-4I has multiple wide optical–optical gaps in the range from 15 THz to 35 THz. Therefore, the decrease of phonon thermal conductivity of Si_2BN-4I compared with Si_2BN results from the decrease of the group velocity.[53]

In order to study the effect of temperature on thermoelectric properties, the TE performance of the armchair direction of Si_2BN-4I at the temperatures of 300 K, 500 K, and 800 K is calculated and shown in Fig. 7. As the temperature increases, the PF of Si_2BN-4I increases (in Fig. 7(c)), while the phonon thermal conductivity of Si_2BN-4I decreases (in Fig. 7(e)). As a result, the ZT value of Si_2BN-4I increases with the increase of temperature (in Fig. 7(f)), and the ZT of Si_2BN-4I can reach 0.8 at 800 K. However, compared with Figs. 7(c) and 7(f), the optimal ZT carrier concentration (N_{ZT}) has a large deviation from the optimal PF carrier concentration (N_{PF}), and the PF corresponding to N_{ZT} is relatively low. Obviously, with the increase of temperature, N_{PF} becomes lower, S corresponding to N_{PF} decreases very slight, and the increase of electrical conductivity σ is also very small. But with the increase of temperature, the increase of κ_e corresponding to N_{PF} is much greater than that of κ_p, and the value of κ_e is an order of magnitude higher than that of κ_p. Therefore, κ_e plays a major role that influences the ZT with the change of temperature, and N_{ZT} moves towards the lower κ_e. This limits the improvement of ZT to some extent, and the excessive κ_e also indicates that there is still space for improvement of the TE performance of Si_2BN-4I.[58]

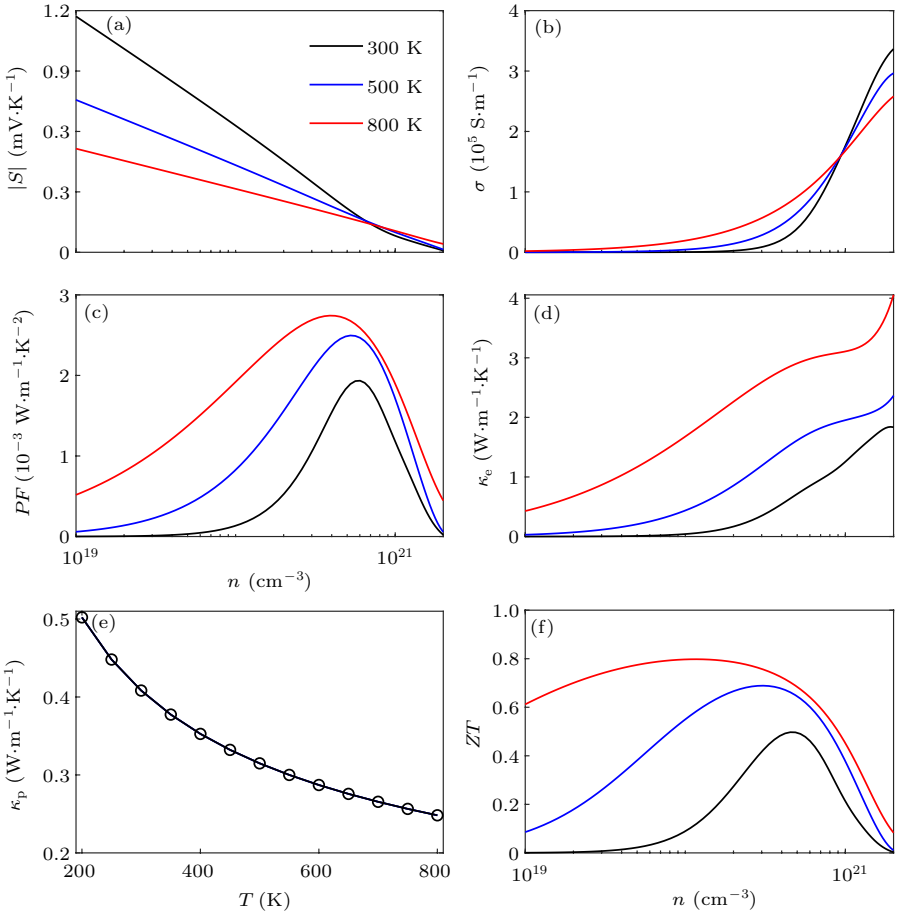


Fig. 7. (a) The Seebeck coefficient, (b) electrical conductivity, (c) power factor, (d) electronic thermal conductivity, (e) phonon thermal conductivity, and (f) ZT of Si_2BN-4I along armchair direction at 300 K, 500 K, and 800 K, respectively.

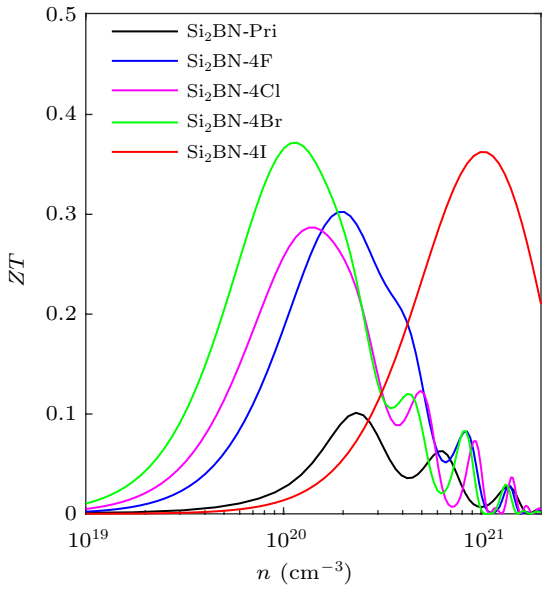


Fig. 8. The ZT of Si_2BN and Si_2BN-4X along zigzag direction at 300 K.

The above calculations of TE properties are based on the armchair direction. In Fig. 8(a), we obtain the ZT values of Si_2BN and Si_2BN-4X at 300 K along the zigzag direction. In the zigzag direction of Si_2BN-4I, we draw the same conclusion as in the armchair direction, but the TE performance in the zigzag direction is slightly lower than that in the armchair direction, so we mainly introduce the TE performance in the armchair direction. The similar conclusions can be obtained in the zigzag direction.

4. Conclusion

In this work, we study the electron transport, thermal transport, and thermoelectric properties of Si_2BN adsorbing halogen atoms (Si_2BN-4X, X = F, Cl, Br, and I) using the first principles calculation and Boltzmann transport theory. The adsorption of halogen atoms can significantly regulate the energy band structure and lattice thermal conductivity of Si_2BN. The band gap of Si_2BN is opened by adsorbing halogen atoms, which leads to the increase of Seebeck coefficient. In particular, Si_2BN-4I has the largest Seebeck coefficient because of the band degeneracy. In addition, the absorption of halogen atoms increases the phonon scattering, and the lattice thermal conductivity decreases significantly, which leads to a significant increase of ZT.

References

[1] Zeng Y J, Wu D, Cao X H, Zhou W X, Tang L M and Chen K Q 2020 *Adv. Funct. Mater.* **30** 1903873
[2] Pei Y Z, Wang H and Snyder G J 2012 *Adv. Mater.* **24** 6125
[3] Jiang P H, Liu H J, Cheng L, Fang D D, Zhang J, Wei J, Liang J H and Shi J 2017 *Carbon* **113** 108

[4] Zhou W X, Cheng Y, Chen K Q, Xie G F, Wang T and Zhang G 2020 *Adv. Funct. Mater.* **30** 1903829
[5] Kovnir K and Toberer E S 2016 *Chemistry of Materials* **28** 2463
[6] Chetty R, Bali A and Mallik R C 2015 *J. Mater. Chem. C* **3** 12364
[7] Wu D, Cao X H, Chen S Z, Tang L M, Feng Y X, Chen K Q and Zhou W X 2019 *J. Mater. Chem. A* **7** 19037
[8] Zhou X Y, Yan Y C, Lu X, Zhu H T, Han X D, Chen G and Ren Z F 2018 *Materials Today* **21** 974
[9] Hatam-Lee S M, Rajabpour A and Volz S 2020 *Carbon* **161** 816
[10] Liang T, Zhang P, Yuan P, Zhai S P and Yang D G 2019 *Nano Futures* **3** 015001
[11] Wang X N and Tabarraei A 2016 *Appl. Phys. Lett.* **108** 191905
[12] Hinterleitner B, Knapp I, Poneder M, Shi Y P, Müller H, Eguchi G, Eisenmenger-Sittner G, Stöger-Pollach M, Kakefuda Y, Kawamoto N, Guo Q, Baba T, Mori T, Ullah S, Chen X Q and Bauer E 2019 *Nature* **576** 85
[13] Zhou W X and Chen K Q 2015 *Sci. Rep.* **4** 7150
[14] Chen X K, Liu J, Peng Z H, Du D and Chen K Q 2017 *Appl. Phys. Lett.* **110** 091907
[15] Xie G F, Ding D and Zhang G 2018 *Advances in Physics: X* **3** 1480417
[16] Xie Z X, Liu J Z, Yu X, Wang H B, Deng Y X, Li K M and Zhang Y 2015 *J. Appl. Phys.* **117** 114308
[17] Xie Z X, Zhang Y, Yu X, Li K M and Chen Q 2014 *J. Appl. Phys.* **115** 104309
[18] Wu D, Cao X H, Jia P Z, Zeng Y J, Feng Y X, Tang L M, Zhou W X and Chen K Q 2020 *Sci. China Phys. Mech. Astron.* **63** 276811
[19] Gu X K, Wei Y J, Yin X B, Li B W and Yang R G 2018 *Rev. Mod. Phys.* **90** 041002
[20] Xu X F, Chen J and Li B W 2016 *J. Phys.: Condens. Matter* **28** 483001
[21] Wang J, Zhu L, Chen J, Li B and Thong JTL 2013 *Adv. Mater.* **25** 6884
[22] Liu Z Y, Wu X F and Luo T F 2017 *2D Mater.* **4** 025002
[23] Sun Y Y, Chen L, Cui L, Zhang Y W and Du X Z 2018 *Computational Materials Science* **148** 176
[24] Xu M, Wang H Y, Sun S S, Li H T, Li X M, Chen Y Z and Ni Y X 2020 *Phys. Status Solidi B* **257** 1900205
[25] Nguyen D K, Tran N T T, Chiu Y H and Lin M F 2019 *Sci. Rep.* **9** 13746
[26] Kishore M R A, Sjåstad A O and Ravindran P 2019 *Carbon* **141** 50
[27] Andriotis A N, Richter E and Menon M 2016 *Phys. Rev. B* **93** 081413
[28] Shukla V K, Araujo R B, Jena N K and Ahuja R 2017 *Nano Energy* **41** 251
[29] Singh D, Gupta S K, Sonvane Y, Hussain T and Ahuja R 2018 *Phys. Chem. Chem. Phys.* **20** 21716
[30] Singh D, Gupta S K, Sonvane Y and Ahuja R 2017 *International Journal of Hydrogen Energy* **42** 22942
[31] Singh D, Chakraborty S and Ahuja R 2019 *ACS Applied Energy Materials* **2** 8441
[32] Yeoh K H, Yoon T L, Ong D S, Lim T L and Abdullahi Y Z 2017 *Phys. Chem. Chem. Phys.* **19** 25786
[33] Kresse G and Furthmuüller J 1996 *Phys. Rev. B* **54** 11169
[34] He Y, Zhang M, Shi J J, Cen Y L and Wu M 2019 *J. Phys. Chem. C* **123** 12781
[35] Deng T Q, Yong X, ShiW, Gan C K, LiW, Hippalgaonkar K, Zheng J C, Wang X B, Yang S W, Wang J S and Wu G 2019 *Adv. Electron. Mater.* **5** 1800892
[36] Zhou W X, Wu D, Xie G F, Chen K Q and Zhang G 2020 *ACS Omega* **5** 5796
[37] Madsen G K and Singh D J 2006 *Comput. Phys. Commun.* **175** 67
[38] Hung N T, Nugraha A R T, Hasdeo E H, Dresselhaus M S and Saito R 2015 *Phys. Rev. B* **92** 165426
[39] Maurya V and Joshi K B 2019 *J. Alloys Compd.* **779** 971
[40] Zhu X L, Liu P F, Zhang J R, Zhang P, Zhou W X, Xie G F and Wang B T 2019 *Nanoscale* **11** 19923
[41] Madsen G K H and Singh D J 2006 *Computer Physics Communications* **175** 67
[42] Wang J, Xie F, Cao X H, An S C, Zhou W X, Tang L M and Chen K Q 2017 *Sci. Rep.* **7** 41418
[43] Gandi A N, Alshareef H N and Schwingenschlögl U 2016 *Chemistry of Materials* **28** 1647
[44] Zhou W X and Chen K Q 2015 *Sci. Rep.* **5** 15070
[45] Zhang Q Q, Jia P Z, Chen X K, Zhou W X and Chen K Q 2020 *J. Phys.: Condens. Matter* **32** 305301
[46] Gu X K and Yang R G 2014 *Appl. Phys. Lett.* **105** 131903
[47] Klemens P G 2000 *J. Wide Bandgap Mater.* **7** 332
[48] Morelli D T, Heremans J P and Slack G A 2002 *Phys. Rev. B* **66** 195304
[49] Chen X K and Chen K Q 2020 *J. Phys.: Condes. Matter* **32** 153002
[50] Mahida H R, Singh D, Sonvane Y, Thakor P B, Ahuja R and Gupta S K 2019 *J. Appl. Phys.* **126** 233104
[51] Peng B, Zhang D Q, Zhang H, Shao H Z, Ni G, Zhu Y Y and Zhu H Y 2017 *Nanoscale* **9** 7397
[52] Wu J, Chen Y B, Wu J Q and Hippalgaonkar K 2018 *Adv. Electron. Mater.* **4** 1800248
[53] Snyder G J and Toberer E S 2008 *Nat. Mater.* **7** 105
[54] Pei Y Z, Shi X Y, LaLonde A, Wang H, Chen L D and Snyder G J 2011 *Nature* **473** 66
[55] Zhao, L D, Dravid V P and Kanatzidis M G 2014 *Energy Environ. Sci.* **7** 251
[56] Yu J B, Li T W and Sun Q 2019 *J. Appl. Phys.* **125** 205111
[57] Kumar S and Schwingenschlögl U 2016 *Phys. Rev. B* **94** 035405
[58] Yu J B, Li, T W, Nie G, Zhang B P and Sun Q 2019 *Nanoscale* **11** 10306